Design of an Autonomous Fast-Walking Humanoid Robot

M HARDT, **O von STRYK**
Simulation and Systems Optimization, Technische Universität Darmstadt, 64283 Darmstadt, Germany
D WOLLHERR, **M BUSS**
Control Systems Group, Technical University Berlin, 10587 Berlin, Germany

This is a preprint of the paper that appeared in:
CLAWAR: International Conference on Climbing and Walking Robots, Paris, France, September 25-27 (Professional Engineering Publishing Ltd., 2000) 391-398.

ABSTRACT

The design considerations for a small, relatively fast walking, autonomous humanoid robot are presented. The robot must be energy efficient but also produce sufficient torque to reach greater speeds. On the basis of previous investigations into gait optimization for multilegged systems, dynamical modeling and nonlinear optimization tools are used for design optimization and choosing the motor size and gear ratios. Gait trajectories for relatively fast steps and different prototypes were calculated. The design decisions are described for the humanoid robot with 6 degrees-of-freedom (DoF) in each leg and 2 DoF in each arm based on numerical results and preliminary investigations with a 4 DoF test robot.

1 INTRODUCTION

This paper presents the design and development strategies of a small-size and fast, autonomous humanoid walking machine. Many research groups investigate biped walking machines where most effort is put into hardware design (1, 7, 9). The actual development and production can be so expensive and time consuming that university research labs have difficulty competing with larger companies (5, 6). The goal in this project is to keep the mechanical construction as simple, cheap, and lightweight as possible. The design concept is kinematically similar to PINO (12) but uses off-the-shelf, high performance DC motors. The robot design should also consist identical mechatronic modules linked together for ease of maintenance.

The autonomous humanoid is intended for fast, dynamic walking; thus, its dynamical behavior is extremely important. Numerical simulation and optimization of full nonlinear dynamic models are used throughout the entire design and control development process. Efficient, recursive multibody dynamic algorithms (4) are particularly well-suited for modeling legged systems. These are combined with powerful nonlinear optimization programs (10) to generate gait trajectories (2, 3) or to optimize kinematic and dynamic model parameters. Using this data, a choice for the motors and gears may be made which deliver the desired performance. The robot design, i.e. trade-off between motor weight and power, are further optimized with respect to a walking speed of approximately 0.5 m/s.

The organization of this paper is as follows. Section 2 describes design considerations based on optimal control solutions of robot steps. Design and experimental results with the 4 DoF prototype robot DONALD are presented in Section 3.

2 DESIGN BASED ON OPTIMAL CONTROL

2.1 Robot Kinematic Structure

A preliminary architecture used for the 70 cm humanoid robot is shown in Figure 1 with dimensions given in Table 1. Each robot leg features 6 DoF: 2 DoF in the ankle allowing for forward and lateral movement, 1 DoF in the knee, and 3 DoF in the hips for a full range of movement. Two DoF are placed in each shoulder to compensate leg momenta with arm swinging and to provide lateral stability. A model for the kinematic structure thus has 16 DoF. For simplicity, the head is fixed to the torso in the model. Two different weight classes were initially considered for the robot: a heavier 18 kg version and a lightweight 12 kg one. The links are modeled with uniformly distributed mass where the massed are listed in Table 2.

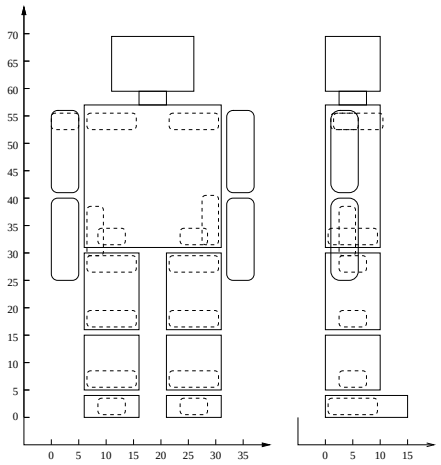

Figure 1: Preliminary Model

Table 1: Link dimensions in local coordinates

	Torso	Thigh	Shank
d_x [m]	0.1	0.14	0.15
d_y [m]	0.25	0.1	0.1
d_z [m]	0.385	0.1	0.1

Table 2: Link masses

Model	Torso	Thigh	Shank
12 kg	7.355	1.161	1.161
18 kg	11.03	1.742	1.742

Other important biped model characteristics were neglected such as an elastic foot damping material for collision absorption, contact at multiple points with a spatial foot, and rolling contact. Instead, point contact of the legs with the ground were modeled in this first study. These dynamic modeling properties will be included in future work for the generation of reference trajectories and control design. The links are also not completely rigid, but slightly flexible and thus must be considered as modeling uncertainties. The additional shock absorption effect provided by the flexibility though is expected to be beneficial.

Table 3: Numerical investigative modeling frameworks

Experimental Model	Weight	Average Forward Speed
Model 1	12 kg	0.417 m/s (1.5 km/h)
Model 2	12 kg	0.555 m/s (2.0 km/h)
Model 3	18 kg	0.417 m/s (1.5 km/h)
Model 4	18 kg	0.555 m/s (2.0 km/h)

2.2 Optimized Walk of a Biped

The biped is optimized over one step where the movement is constrained to the sagittal plane. Each leg instantaneously lifts off from the ground when the other collides with the ground representing the most efficient form of walking without feet. The leg collision with the ground is modeled as perfectly inelastic, i.e. the leg tip velocity is instantaneously zero after collision.

The dynamical model is that of a rigid, multibody system experiencing contact forces:

$$\begin{aligned} \ddot{\mathbf{q}} &= \mathcal{M}(\mathbf{q})^{-1}\Big(B\mathbf{u} - \mathcal{C}(\mathbf{q},\dot{\mathbf{q}}) - \mathcal{G}(\mathbf{q}) + J_c(\mathbf{q})^T\mathbf{f}_c\Big) \\ 0 &= \mathbf{g_c}(\mathbf{q}) \end{aligned} \tag{2.1}$$

where $\mathcal{M}$ is the positive-definite mass-inertia matrix, $\mathcal{C}$ is the Coriolis and centrifugal force vector, $\mathcal{G}$ the gravitational force vector, $\mathbf{q}$ the generalized coordinates, and $\mathbf{u}(t)$ are the control inputs mapped with the constant matrix B to the actively controlled joints. The constraint Jacobian $J_c = \frac{\partial \mathbf{g_c}}{\partial \mathbf{q}}$ is obtained from the holonomic ground contact constraints $\mathbf{g_c}$, and $\mathbf{f}_c$ is the ground contact force. These equations are evaluated using recursive, multibody algorithms which are arguably the most efficient numeric approach for calculating such high-dimensional dynamics (3). Other advantages are that parameters are easily adapted to changes in the model.

With the goal of an autonomous, fast-moving biped, a performance measure is chosen that minimizes energy loss. It is known that the principal form of energy loss for these systems is Joule thermal loss (8). As almost identical motors are sought for all joints for ease of maintenance and repair, this measure can be expressed as the integral of the squared applied forces. An additional constraint is also imposed on the maximum power consumption M_W for each motor. Let $\dot{q}_i$ be the joint i angle velocity, n the total number of links. Then the optimal control problem subject to the robot dynamics (2.1) is:

$$\min_{\mathbf{u}} \left\{ \int_0^{t_f} \mathbf{u}(t)^T\mathbf{u}(t)\,\mathrm{d}t \right\} \qquad \text{subject to} \qquad \max_{t\in[0,t_f],i\in\{1,\ldots,n\}} |\dot{q}_i(t)u_i(t)| \le M_W \tag{2.2}$$

Four different models were used to investigate the torque and power requirements for dynamic walking as shown in Table 3. Optimal control problems were solved numerically using the method of direct collocation based on a parameterization of state and control variables using piecewise polynomials and its solution with sparse, large-scale sequential quadratic programming (3, 10). In spite of the wide range of power, torque, and speed output characteristics present in commercial high performance motors, a significant void generally exists between motors with a 20–25 W maximum power output and those with a 70 W max power output, the latter having a much increased weight. For this reason, both Models 1 & 2 were optimized

Table 4: Model 2 (0.555 m/s, 12 kg): Max. vertical contact force = 187 Nm

Velocities	H1	K1	H2	K2
Aver. (rpm)	19.7	14.4	53.8	62.0
Max. (rpm)	81.7	102	99.8	127
Accelerations	H1	K1	H2	K2
Max. (rad/s^2)	409	515	318	323
Torques	H1	K1	H2	K2
Aver. (Nm)	1.54	1.95	0.947	0.299
Max. (Nm)	5.67	4.21	1.71	0.993
Power	H1	K1	H2	K2
Aver. (W)	3.50	3.51	5.80	2.13
Max. (W)	15.4	23.1	13.9	6.02

Table 5: Model 4 (0.555 m/s, 18 kg): Max. vertical contact force = 269 Nm

Velocities	H1	K1	H2	K2
Aver. (rpm)	19.8	14.4	54.6	62.8
Max. (rpm)	83.8	105	101	126
Accelerations	H1	K1	H2	K2
Max. (rad/s^2)	731	815	485	538
Torques	H1	K1	H2	K2
Aver. (Nm)	2.29	2.95	1.36	0.42
Max. (Nm)	8.05	6.16	2.38	1.40
Power	H1	K1	H2	K2
Aver. (W)	5.32	5.60	8.47	3.07
Max. (W)	27.3	41.9	20.2	9.05

with a joint maximum power output of M_W = 20 W as in (2.2). The problem was not solvable in this form for Models 3 & 4 most likely due to the fact that the forward velocity constraints could not be met with the increased weight and limited power availability. M_W was thus set higher for the heavier models: M_W = 25 W for Model 3, M_W = 40 W for Model 4.

An optimal control problem for one walking step is solved numerically for each model resulting in solution trajectories of joint velocities, accelerations, applied torques, and required power. The results for models 2 & 4 are displayed in Tables 4 & 5 with the notation: (Hi) = Leg i Hip; (Ki) = Leg i Knee. Leg 1 is the support leg and Leg 2 is the swing leg. The power maxima indicated in these tables may be slightly above the upper bound above due to polynomial approximations between calculated grid points. The most important conclusion that the data provides is that required power increases at a rate faster than linear with respect to the overall system weight. The larger motors with greater power outputs in turn weigh much more so that system weight quickly spirals upward making the construction of a system capable of fast movements increasingly difficult. Thus, a strong effort was made to maintain the total biped weight small.

Figures 2 & 3 display various trajectories for the four models M1–M4. Spikes in the torque and speed trajectories are a consequence of the model and the high average forward velocity. These occur near the time of collision of the leg with the ground. A well-designed foot construction including damping elements should avoid these peaks; therefore, they are neglected in the motor selection process. A foot will permit the biped to make larger and fewer steps thus reducing the predicted high values for the joint velocities. The relationship between the maximum required motor torque and its turning speed is also shown in Fig. 3. We summarize the data of interest in Table 6 to be used for motor selection.

2.3 Motor Selection

The task of drive selection is to find a drive train satisfying the desired characteristics in Table 6. The maximum power ratings and required torque lead to the preliminary selection of a Maxon RE25, 20W motor and Maxon GP32A gear, though the voltage rating and gear ratio need to be to determined. The Maxon motor was chosen because of the high torque to weight

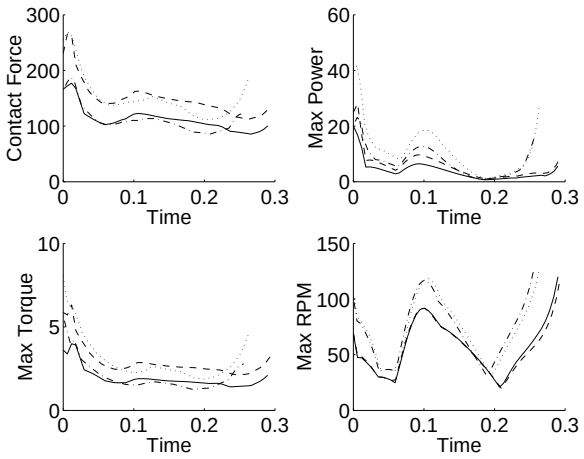

Figure 2: M1: solid line, M2: dashdot, M3: dashed, M4: dotted

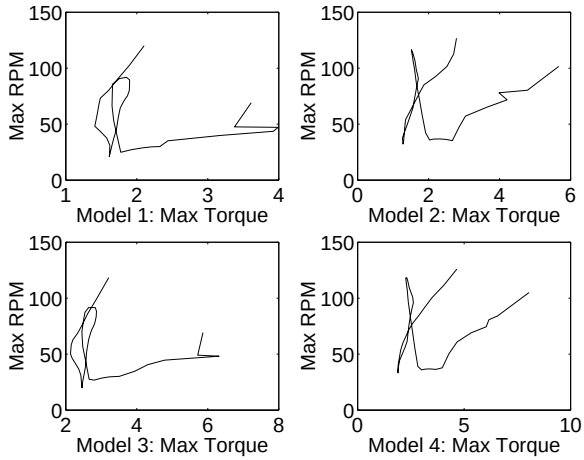

Figure 3: Torque vs RPM

Table 6: Motor characteristics for the 12 and 18 kg models.

	12 kg model	18 kg model
Operational torque:	1.5–2.5 Nm	2.5–3.5 Nm
Maximum torque:	3.0 Nm	4.0 Nm
Operational RPM:	50–75 rpm	65–90 rpm
Maximum RPM:	90 rpm	100 rpm
Maximum Power:	15 W	20 W

ratio in comparison with other manufacturers.

Figures 4 & 5 display required motor torques against rpm from Models 2 & 4 respectively. The required motor torques T_m are calculated from the chosen gear ratio N_i and efficiency h_i

$$T_m = \frac{T}{N_i \, h_i} \tag{2.3}$$

while the required motor speed n_r is obtained from the gear output speed n_o and gear ratio

$$n_r = n_o N_i \ . \tag{2.4}$$

Additionally plotted for each given gear ratio are three different motor voltage ratings: $V_m = \{30\text{V}, 42\text{V}, 48\text{V}\}$ assuming a battery supply voltage of $V_s = 38\text{V}$ delivered by three batteries providing 14.4 V each. The motor characteristic lines in Figs. 4 & 5 are calculated by first determining the no-load motor speed n_{mV} from its rated value n_m and adjusted according to the supply voltage V_s

$$n_{mV} = n_m \frac{V_s}{V_m}. \tag{2.5}$$

The given slope of each motor characteristic line determines the reachable torque and velocity combinations as the set of all points below the line. The desired workspace of the motor thus should lie beneath this line.

In Fig. 5, the desired workspace is not covered as well by the motor characteristic lines as with the 12 kg robot. The heavier robot will not be able to be driven nearly as fast as the lighter one; a traveling speed of 0.417 m/s though is still achievable. The best choice appears to be a 42V motor with a 66:1 gear ratio.

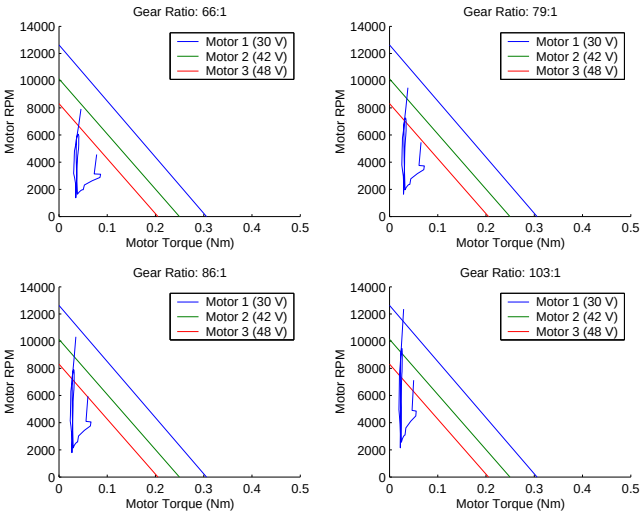

Figure 4: Model 2: Motor torque vs. rpm

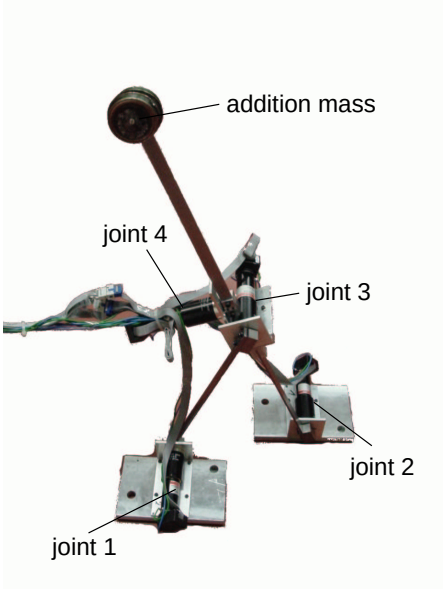

Figure 6: DONALD, side view

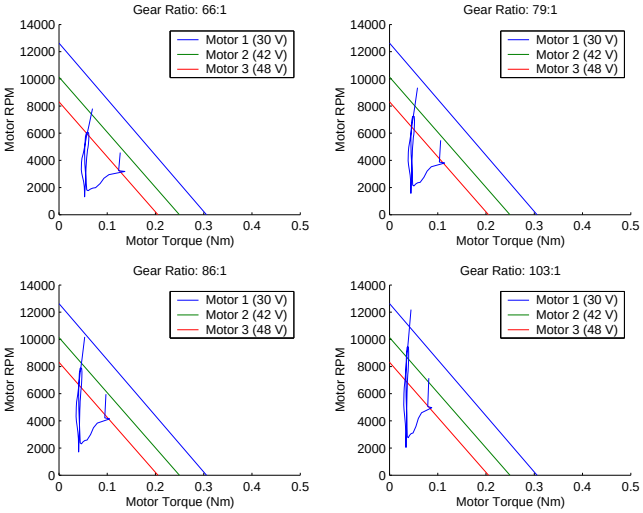

Figure 5: Model 4: Motor torque vs. rpm

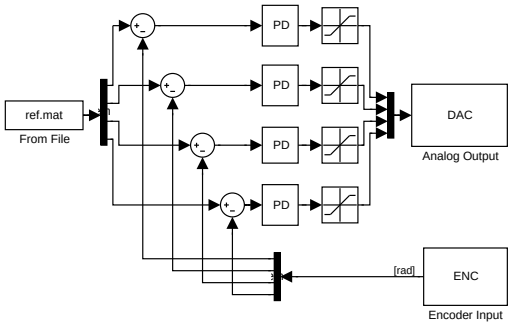

Figure 7: SIMULINK control

3 FOUR DoF PROTOTYPE WALKER DONALD

A first test platform with 4 DoF has been built to test the motors and control architecture. The prototype walking robot DONALD is a highly simplified version of the humanoid robot described in Section 2 lacking the upper part of the body and knees.

As shown in Fig. 6, DONALD consists of four identical, serially linked joints. At each joint the shaft of the motor is fixed to an L-shaped base plate and the axis of the motor to a lever arm. The far end of the lever arm is then connected to the base plate of the next joint. With these elementary joint modules, a walking robot has been constructed featuring two legs, no knees and feet with a 1 DoF ankle joint. As the orthogonal projection of the center of mass to the floor can always be located between DONALD's feet, statically stable walking is easily implemented. To achieve this an additional mass was added at the top of a 1 DoF inverted pendulum with

Table 7: Physical parameters of DONALD.

link length l	280 mm
mass of each link	103 g
size of footplate	$(100 \times 160)\mathrm{mm}^2$
mass of footplate	570 g
mass of motor, gear, encod.	376 g
gear ration	246:1
mass of base plate	137 g

its center of rotation at the hips and oriented orthogonally to the walking direction. After each step, this mass is shifted to the other side in order to relocate the the center of mass over the support leg. The physical parameters of DONALD are shown in Table 7.

The motors are all equipped with pulse encoders. The data is processed by a PC based Sensoray 626 multifunction I/O board providing D/A conversion and quadrature decoders. The D/A conversion channels are used to drive the motor through a pulse-width-modulator (PWM) amplifier which provides the necessary power. Using the quadrature decoders, the actual position and velocity is determined allowing to implement a closed loop control for trajectory following. This infrastructure was initially provided externally using cabling. The next prototype's motors will be accessed using a Motorola microcontroller MC68HC908BD48 which receives the desired control input from an onboard PC by USB connection and generates the corresponding PWM signal driving a MOSFET H-bridge.

The real-time capable rapid prototyping software environment developed in the Control Systems Group in Berlin (11) is implemented. Additionally Real-Time (RT) Linux is chosen as the onboard operating system. The MATLAB Real-time Workshop permits the generation and compilation of standalone real-time code for RT Linux from a SIMULINK model. The control loop to be implemented is composed of ordinary SIMULINK block-sets, hence the migration from designing a controller in offline mode to evaluating it in an experiment is subject to substituting the system model by hardware in the loop which can also be accessed through SIMULINK block-sets.

Using heuristically determined trajectories for the joint angles, Fig. 7 shows the rather simple SIMULINK block diagram implementing this PD position control loop. One important outcome of these investigations was to ascertain the stiffness of the construction. The apprehension that the construction is too lightweight and not stiff enough could be discounted. Even with significant accelerations from various body parts, the links between the joints are stiff enough to prevent vibrations and oscillations due to link resonances. Also the legs do not significantly bend when hitting an obstacle.

4 CONCLUSIONS AND OUTLOOK

In this paper the first steps towards the design of a new, autonomous walking robot with 16 DoF have been presented. Detailed numerical simulation and optimization of motion dynamics is used in each step of the design and control development process. On this basis, the motor selection was made. The simplified 4 DoF prototype DONALD was used to separately test newly developed components of the robot and the motors before actually integrating them into

the full DoF walking machine.

The next steps will include foot design and a dynamical analysis of the 16 DoF biped (in the sagittal plane and also in three dimensions) with swinging arms for improving stability and walking speed. In further steps, the development of feedback controllers will be developed based on real-time software-in-the-loop simulations using full multibody dynamical models, motor and gear dynamics as well as models for foot-ground contact and sensors. Its future participation in the robot world soccer championships (RoboCup) is planned, where not only fast dynamic movement but also real-time perceptive and reaction capabilities with the environment are necessary.

REFERENCES

(1) T. Arakawa and T. Fukuda, "Natural Motion Generation of Biped Locomotion Robot using Hierarchical Trajectory Generation Method Consisting of GA, EP Layers," in *IEEE International Conf. on Robotics and Automation*, (Albuquerque, New Mexico) (1997) 211–216

(2) Hardt, M.; Helton, J.W.; Kreutz-Delgado, K.: "Optimal Biped Walking with a Complete Dynamical Model," *IEEE Conference on Decision and Control* (1999) 2999–3004

(3) M. Hardt and O. von Stryk, "The role of motion dynamics in the design, control and stability of bipedal and quadrupedal robots," in *RoboCup 2002 International Symposium* (Fukuoka, Japan) (2002)

(4) Helm, A.; Hardt, M.; Höpler, R.; von Stryk, O.: "Development of a Toolbox for Model-Based Real-Time Simulation and Analysis of Legged Robots," GAMM Conference (Augsburg, Germany) (2002)

(5) K. Hirai, M. Hirose, Y. Haikawa, and T. Takenaka, "The Development of Honda Humanoid Robot," in *IEEE International Conference on Robotics and Automation*, (Leuven, Belgium) (1998) 1321–1326

(6) M. Hirose, Y. Haikawa, T. Takenaka, and K. Hirai, "Development of Humanoid Robot ASIMO," in *IEEE/RSJ International Conference on Intelligent Robots and Systems (IROS) – Workshop 2*, (Maui, Hawaii) (2001)

(7) M. Inaba, T. Igarashi, S. Kagami, and H. Inoue, "A 35 DOF Humanoid that can Coordinate Arms and Legs in Standing up, Reaching and Grasping an Object," in *IEEE/RSJ Intern'l Conf. on Intelligent Robots and Systems (IROS)*, (Osaka, Japan) (1996) 29–36

(8) H. Kimura, I. Shimoyama, H. Miura, "Dynamics in the dynamic walk of a quadruped robot," *Advanced Robotics* **4**(3) (1990) 283–301

(9) J. Laci, H. Hooshang, and C. Bradley, "A Control Strategy for Adaptive Bipedal Locomotion," in *IEEE International Conf. on Robotics and Automation*, (Minneapolis, Minnesota) (1996) 563–569

(10) O. von Stryk, "User's Guide for DIRCOL Version 2.1," Simulation and Systems Optimization Group, Technische Universität Darmstadt (`www.sim.informatik.tu-darmstadt.de/sw/dircol/`)

(11) D. Wollherr and M. Buss, "Cost Oriented VR-Simulation Environment for Computer Aided Control Design," in *Proceedings of the 6th IFAC Symposium on Cost Oriented Automation*, (Berlin, Germany) (2001)

(12) F. Yamasaki, T. Miyashita, T. Matsui, and H. Kitano, "PINO the Humanoid : A basic Architecture," in *4th International RoboCup Symposium*, (Melbourne, Australia) (2000)